Available online at www.sciencedirect.com
SCIENCE DIRECT®
International Journal of Heat and Mass Transfer 47 (2004) 4525–4533
International Journal of HEAT and MASS TRANSFER
www.elsevier.com/locate/ijhmt

Effect of high frequency magnetic field on CZ silicon melt convection

Tetsuo Munakata [a,*], Satoshi Someya [a], Ichiro Tanasawa [b]

[a] *Institute for Energy Utilization, National Institute of Advanced Industrial Science and Technology, 1-2-1 Namiki, Tsukuba, Ibaraki 305-8564, Japan*

[b] *Department of Mechanical Engineering, Nihon University, Tamura-cho, Kooriyama, Fukushima 963-8642, Japan*

Received 15 May 2003
Available online 11 June 2004

Abstract

Melt flow structure during the silicon single crystal growth process strongly affects the crystal quality. Therefore, melt convection control technique should be developed to obtain the high quality single crystal. For this purpose, we proposed a high frequency magnetic field applied method, and numerically investigated the effect of high frequency magnetic field on Czochralski (CZ) silicon melt convection. The results revealed that the melt convection was strongly affected by the applied electric current and frequency. The temperature distribution just below the crystal became flat if the applied electric current and frequency were selected as optimized value.

1. Introduction

Silicon single crystal is commonly used as a semiconductor material and is the most important material in the semiconductor industry. To obtain such single crystals, melt growth technique, i.e., Czochralski (CZ), Floating Zone (FZ) and/or Bridgman methods, is widely used. On the melt growth technique, the quality of single crystal is strongly affected by the melt convection [1,2]. The melt convection structure is governed by the simultaneously acting forces [3–11], i.e., buoyancy force [12], surface tension [13–18], crystal/crucible rotation [19] and so on. Therefore, melt convection control technique should be developed to obtain the high quality crystal. For this purpose, magnetic field applied methods are considered up to now, i.e., vertical, transverse and cusp DC magnetic fields [20–27] and/or rotational magnetic field [28,29]. These methods have a dumping or stabilizing effect for the melt convection, and it is useful to produce a crystal stably. However, the temperature and concentration fields are dominated by conduction, resulting in the inhomogeneous impurity concentration distribution in the crystal in the radial direction. To avoid this tendency, Watanabe et al. recently proposed the electromagnetic CZ (EMCZ) method [30,31]. In this method, vertical DC magnetic field and transverse electric current were applied simultaneously; the melt was stirred due to the induced Lorentz force and the concentration distribution became flat in the radial direction. Therefore, we must develop the melt convection control technique not only for the suppression technique but also the enhancement technique.

Witzel et al. [32] and Virbulis et al. [33] considered the effect of AC magnetic field on the melt convection and found that the melt flow structure could be change by the AC magnetic field. Unfortunately, they only considered the 50 Hz of AC magnetic field. Since the melt flow structure is influenced by the applied frequency and the coil position, we must investigate these effects to optimize the magnetic field for the CZ crystal growth process. In the previous papers [34,35], we proposed a high frequency magnetic field applied method to

* Corresponding author. Fax: +81-29-851-7523.
E-mail address: t.munakata@aist.go.jp (T. Munakata).

0017-9310/$ - see front matter © 2004 Elsevier Ltd. All rights reserved.
doi:10.1016/j.ijheatmasstransfer.2003.06.009

Nomenclature

C_p	specific heat (J/kg K)
EM_1	dimensionless electromagnetic parameter $= \mu_e^2 J_\theta^2 \sigma_e \omega_e R_c^6/(2\rho_0 \nu^2)$
EM_2	dimensionless electromagnetic parameter $= \mu_e^2 J_\theta^2 \sigma_e \omega_e^2 R_c^6/(2\rho_0 \nu C_p \Theta_m)$
EM_3	dimensionless electromagnetic parameter $= \mu_e \sigma_e \omega_e R_c^2$
EM_4	dimensionless electromagnetic parameter $= \mu_e J_\theta^2 R_c^4/(2\mu\nu)$
g	gravitational acceleration (m/s^2)
H	dimensionless melt height
J_θ	applied coil electric current density (A/m^2)
Ma	Marangoni number $= \sigma_T \Theta_m R_c/(\alpha\mu)$
Pr	Prandtl number $= \nu/\alpha$
Ra	Rayleigh number $= g\beta_T \Theta_m R_c^3/(\alpha\nu)$
R_c	radius of crucible (m)
Rd	radiation number $= \varepsilon\sigma_{SB} R_c \Theta_m^3/\lambda$
R_{ii}, R_{io}	dimensionless inter and outer radius of induction coil
R_s	dimensionless radius of crystal
R_w, Z_w	dimensionless computation domain
R_{wc}	induction coil position
r, z	coordinate
T	dimensionless temperature
t	dimensionless time
V_r, V_z	dimensionless velocity component
Z_{cl}, Z_{cu}	dimensionless lower and upper position of crucible
Z_{il}, Z_{iu}	dimensionless lower and upper position of induction coil
α	thermal diffusivity (m^2/s)
β_T	volumetric expansion coefficient (1/K)
$\delta(R_{wc})$	function which express the induction coil position $= 1$ for induction coil position $= 0$ for the other position
ε	emissivity
φ	modified dimensionless vector potential respect to azimuthal component
λ	thermal conductivity (W/m K)
μ	dynamic viscosity (Pa s)
μ_e	permeability (H/m)
ν	kinematic viscosity (m^2/s)
Θ_m	melting temperature (K)
ρ_0	density (kg/m^3)
σ_e	electrical conductivity (S/m)
σ_{SB}	Stefan–Boltzmann constant (W/m^2 K^4)
σ_T	temperature coefficient of surface tension (N/m K)
ω	dimensionless vorticity
ω_e	angular frequency (rad/s)
ψ	dimensionless stream function

Subscripts

c, s	cosine and sine component
a, b, w	ambient, bottom and side wall, respectively

control the FZ silicon melt convection, and the effect was numerically investigated under the radiation heating. The results revealed that the high frequency magnetic field dramatically affected the melt flow structure and the intensity. On the FZ method, the melt convection is almost governed by the Marangoni convection, which is acting at the melt free surface. The electromagnetic force induced by the high frequency magnetic field is also acting near the melt free surface, i.e. skin depth. If the induction coil is placed at the suitable position and the suitable induction coil current and frequency are selected, the Marangoni force can be eliminated completely. Further, if the induction coil current is increased more, the convection intensity is increased oppositely compared with the natural convection. From these results, the high frequency magnetic field applied method can also be used to control the melt convection for both the suppression and enhancement of the convection intensity.

In this study, we have extended the high frequency magnetic field applied method to the CZ silicon crystal growth process, and numerically investigated the effect of high frequency magnetic field on the CZ silicon melt convection by changing the applied induction coil current and frequency.

2. Numerical procedure

2.1. Governing equations and boundary conditions

The model for CZ crystal growth furnace is schematically illustrated in Fig. 1. In this analysis, the following assumptions are used: (1) the system is axisymmetric, (2) the crystal-melt interface and the melt free surface are flat, (3) the induction coil is one-turn with rectangular cross section and placed at the slightly above the melt free surface, (4) the crystal and crucible are not rotated, and (5) the induced electromagnetic field is not modified by the melt convection. Then the following governing equations and the boundary conditions are obtained in dimensionless form [34,35].

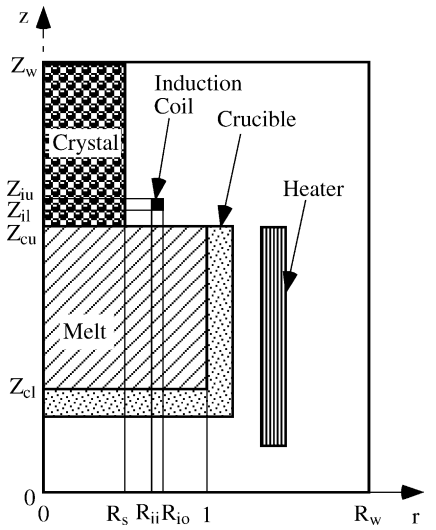

Fig. 1. Schematic model for numerical simulation.

(a) The momentum equation

$$\frac{\partial\omega}{\partial t}+V_r\frac{\partial\omega}{\partial r}+V_z\frac{\partial\omega}{\partial z}-\frac{2V_r}{r}\omega = \frac{\partial^2\omega}{\partial r^2}+\frac{\partial^2\omega}{\partial z^2}-\frac{1}{r}\frac{\partial\omega}{\partial r}-\frac{Ra}{Pr}r\frac{\partial T}{\partial r} - 2\mathrm{EM}_1\frac{1}{r}\left\{\left(\frac{\partial\varphi_c}{\partial r}\frac{\partial\varphi_s}{\partial z}-\frac{\partial\varphi_s}{\partial r}\frac{\partial\varphi_c}{\partial z}\right) -\frac{1}{r}\left(\varphi_c\frac{\partial\varphi_s}{\partial z}-\varphi_s\frac{\partial\varphi_c}{\partial z}\right)\right\} \quad (1)$$

(b) The energy equation

$$\frac{\partial T}{\partial t}+V_r\frac{\partial T}{\partial r}+V_z\frac{\partial T}{\partial z}=\frac{1}{Pr}\left(\frac{\partial^2 T}{\partial z^2}+\frac{\partial^2 T}{\partial r^2}+\frac{1}{r}\frac{\partial T}{\partial r}\right) + \mathrm{EM}_2\frac{1}{r^2}(\varphi_c^2+\varphi_s^2) \quad (2)$$

(c) The stream function (Poisson) equation

$$\frac{\partial^2\psi}{\partial r^2}+\frac{\partial^2\psi}{\partial z^2}-\frac{1}{r}\frac{\partial\psi}{\partial r}=\omega \quad (3)$$

(d) The induction equation

$$\frac{\partial^2\varphi_c}{\partial r^2}+\frac{\partial^2\varphi_c}{\partial z^2}-\frac{1}{r}\frac{\partial\varphi_c}{\partial r}=\mathrm{EM}_3\varphi_s \quad (4)$$

$$\frac{\partial^2\varphi_s}{\partial r^2}+\frac{\partial^2\varphi_s}{\partial z^2}-\frac{1}{r}\frac{\partial\varphi_s}{\partial r}=-\mathrm{EM}_3\varphi_c-r\delta(R_{wc}) \quad (5)$$

(e) The stream function–velocity relation

$$V_r=\frac{1}{r}\frac{\partial\psi}{\partial z},\quad V_z=-\frac{1}{r}\frac{\partial\psi}{\partial r} \quad (6)$$

The boundary conditions:

(f) At the computational boundary ($r=0$, R_w and $z=0$, Z_w)

$$\varphi_c=0,\quad \varphi_s=0 \quad (7)$$

(g) At the center ($r=0$)

$$\omega=0,\quad \psi=0,\quad \partial T/\partial r=0 \quad (8)$$

(h) At the bottom crucible ($z=Z_{cl}$)

$$\omega=\partial^2\psi/\partial z^2,\quad \psi=0,\quad T=T_b+(T_w-T_b)(r/R_c)^2 \quad (9)$$

(i) At the crystal-melt interface ($z=Z_{cu}$, $r=0$ to R_s)

$$\omega=\partial^2\psi/\partial z^2,\quad \psi=0,\quad T=1 \quad (10)$$

(j) At the melt free surface ($z=Z_{cu}$, $r=R_s$ to 1)

$$\omega=-\frac{Ma}{Pr}r\frac{\partial T}{\partial r}+\mathrm{EM}_4\frac{1}{r}\left(\frac{\partial\varphi_c}{\partial r}\frac{\partial\varphi_c}{\partial z}+\frac{\partial\varphi_s}{\partial r}\frac{\partial\varphi_s}{\partial z}\right),$$

$$\psi=0,\quad \frac{\partial T}{\partial r}=-Rd(T^4-T_a^4) \quad (11)$$

(k) At the side crucible ($r=1$, $z=Z_{cl}$ to Z_{cu})

$$\omega=\partial^2\psi/\partial r^2,\quad \psi=0,\quad T=T_w \quad (12)$$

2.2. Numerical method

Above described governing equations with the boundary conditions were solved by the finite difference scheme. In this analysis, the electromagnetic field does not change with time; then the electromagnetic field was calculated at first in the computational domain. The steady-state conduction in the melt, which was calculated by the heat conduction equation with the boundary condition of temperature, was calculated and used as an initial condition for the calculation of melt convection. After that, the melt convection was calculated with time. The computational domain was set as $R_w=6$, $Z_w=12$, $R_s=0.5$, $R_{ii}=0.6$, $R_{io}=0.7$, $Z_{cl}=5.2$, $Z_{cu}=6.2$, $Z_{il}=6.4$ and $Z_{iu}=6.5$, respectively in Fig. 1. The governing equations (1)–(6) were discretized by the second-order central difference for the space and the third-order up-wind difference [36] for the convective terms. The time integration was performed by the ADI method and the Poisson equation was solved by the SOR method. To achieve a high accuracy, following coordinate transformation was used in which the grid points become dense at the boundary.

$$\xi=0.2[\mathrm{Erf}\{10r\}+\mathrm{Erf}\{10(r-0.6)\}+\mathrm{Erf}\{10(r-1.0)\}]+0.1r+0.4 \quad (13)$$

$$\eta=0.2[\mathrm{Erf}\{10(z-5.2)\}+\mathrm{Erf}\{10(z-6.2)\}+\mathrm{Erf}\{10(z-6.4)\}]+0.1z+0.6 \quad (14)$$

where Erf{ } is the Error function. The melt region was divided into 200×200 grids. The used grid system is

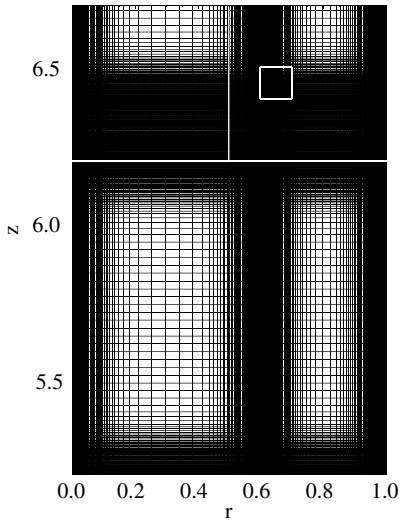

Fig. 2. Grid system for the CZ analysis.

Table 1
Physical properties of silicon

$C_p = 1.0 \times 10^3$ J/kg K	$\nu = 3.0 \times 10^{-7}$ m^2/s
$\alpha = 2.65 \times 10^{-5}$ m^2/s	$\Theta_m = 1680$ K
$\beta_T = 1.4 \times 10^{-4}$ 1/K	$\rho_0 = 2530$ kg/m^3
$\varepsilon = 0.3$	$\sigma_e = 1.2 \times 10^6$ S/m (liquid)
$\lambda = 67.0$ W/m K	5.0×10^4 S/m (solid)
$\mu = 7.59 \times 10^{-4}$ kg/m s	$\sigma_T = 1.0 \times 10^{-4}$ N/m K
$\mu_e = 1.2566 \times 10^{-6}$ H/m	$R_c = 1.0 \times 10^{-2}$ m

shown in Fig. 2 by enlarging near the melt region. The physical properties of silicon are listed in Table 1. The value of the dimensionless parameters were selected as $Pr = 0.011$, $Ra = 2.91 \times 10^5$, $Ma = 8.36 \times 10^4$ and $Rd = 3.21 \times 10^{-2}$ from Table 1. The dimensionless electromagnetic parameters $EM_1 - EM_4$ were changed to obtain the effect of high frequency magnetic field on the melt convection. The temperatures which appeared in boundary conditions are selected as $T_a = 0.9$, $T_b = 1.014881$ and $T_w = 1.020833$, respectively. The computations were performed on the COMPAQ DS20E workstation.

3. Results and discussion

To examine the numerical scheme, the natural convection induced in the CZ silicon melt for various melt height without the high frequency magnetic field are considered first. The results are shown in Fig. 3 for $t = 0.01$. In this figure, the left hand side indicates the flow field (stream line) and the right hand side indicates the temperature field (isotherms). In addition, on the flow field, solid line shows the clockwise flow direction. In the case of $H = 2$, the flow field is mainly circulating in the lower part of the melt and the flow circulation in the upper part is weak. If the melt height is decreased and becomes $H = 1$, the upper melt circulation disappears but the center of the melt flow circulation still exists at lower position. Further, if the melt height becomes $H = 0.5$, the convection cell prevails in the whole melt region and the center of the cell relatively ap-

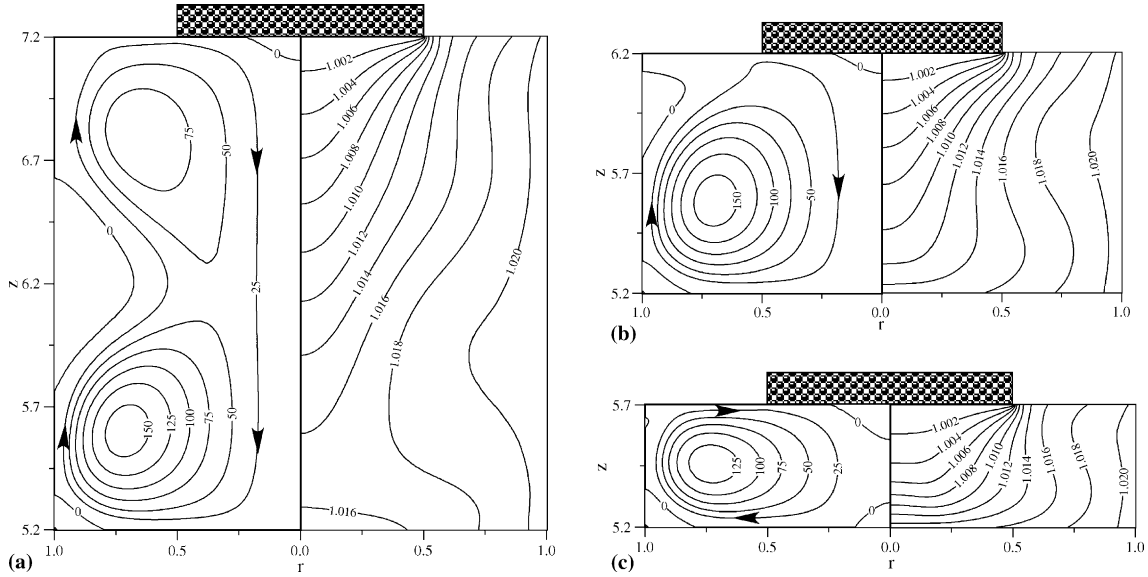

Fig. 3. Flow and temperature fields in the CZ silicon melt under the natural convection for various melt height ($t = 0.01$): (a) $H = 2$; (b) $H = 1$ and (c) $H = 0.5$.

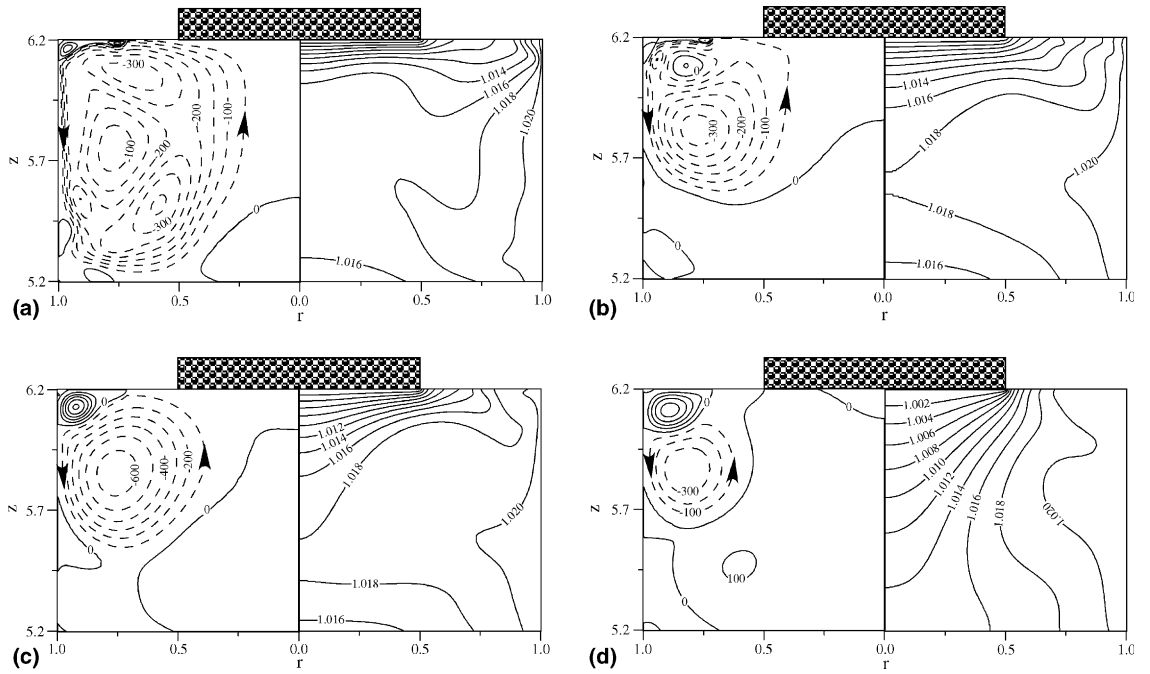

Fig. 4. Effect of applied frequency on the flow and temperature fields in the CZ silicon melt under the applied induction coil current of 216 A ($t = 0.01$): (a) 100 kHz; (b) 300 kHz; (c) 500 kHz and (d) 3 MHz.

proaches to the melt free surface. In every case, clockwise direction flow is induced in the CZ silicon melt by the natural convection. The temperature field, which is usually affected by the flow field, is slightly modified from the heat conduction in every height due to the low Prandtl number fluid. Thus, it can be predicted that the crystal will be grown up as convex toward the melt from the indicated isotherm just below the crystal. The obtained flow structure is different from the result for high Prandtl number fluid [37], however, the tendency of these flow and temperature fields is consistent with the result for low Prandtl number fluid [38]. Therefore, the numerical scheme, which used here, seems valid.

Although the melt flow structure changes with melt height as described above, only the case of $H = 1$ is considered in the following part to simplify the effect of high frequency magnetic field on the natural convection of melt. To examine the effect of high frequency magnetic field on the melt convection, effects of applied frequency and applied current, which are the control parameters, must be considered if the induction coil position is fixed. Then, the effect of applied frequency on the melt convection is considered at first. Fig. 4 shows the effect of applied frequency on the flow and temperature fields in the CZ silicon melt under the fixed applied induction coil current of 216 A. In addition, these figures are obtained for $t = 0.01$, and the dashed line on the flow field indicates the counterclockwise flow direction. As shown in this figure, the flow and temperature fields are completely different from the natural convection, which means that the high frequency magnetic field affects the flow and temperature fields dramatically. Fig. 5 shows an example of electromagnetically induced force distribution in the melt under the high frequency magnetic field of 3 MHz with 216 A. As shown in this figure, electromagnetically induced force is concentrated near

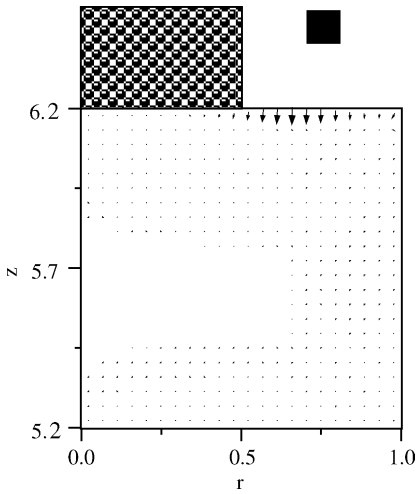

Fig. 5. Electromagnetically induced force distribution under the high frequency magnetic field (3 MHz, 216 A).

the free surface. If the lower frequency of the magnetic field is applied, the skin depth becomes thick and the effect penetrates into much deep region. This will cause the increment of melt mixing effect. This tendency can be seen in Fig. 4. At the lower frequency (Fig. 4(a) and (b)), the whole melt region is governed by the electromagnetically induced convection which has complicated flow structure due to the strong mixing effect. If the applied frequency is increased (Fig. 4(c) and (d)), the flow field becomes rather simple. At the higher frequency, clockwise flow (solid line) is obviously indicated at the free surface near the crucible wall and the counter clockwise flow (dashed line) is indicated below the clockwise convection cell. However, the region of the counterclockwise convection becomes small by increasing the frequency and the melt below the crystal becomes stationary if the applied frequency is reached to 3 MHz. The flow direction separation point at the free surface is located just below the induction coil position. The clockwise convection is also induced by the buoyancy and the Marangoni forces, however, the clockwise convection can not be seen obviously in the lower frequency applied cases. Therefore, it can be considered that both the buoyancy and the Marangoni forces are weak compared with the induced electromagnetic force and the clockwise convection cell indicated in (c) and (d) is originated by the electromagnetic force. The temperature field is strongly affected by this flow structure. The temperature distribution below the crystal becomes almost flat if the applied frequency is less than 500 kHz. However, the temperature distribution below the crystal becomes almost the same as the heat conduction solution at the applied frequency of 3 MHz since the melt becomes stationary at this frequency. Fig. 6 shows the melt temperature variation beneath the center of the crystal. The temperature is strongly fluctuating under the lower applied frequency, however, such fluctuation disappears under the higher frequency and the value reaches to the natural convection value where N.C. indicates the temperature variation under the natural convection. In addition, the counterclockwise convection below the crystal is also induced by the crystal rotation. Then, the high frequency magnetic field has almost the same effect as the crystal rotation at a certain applied frequency. However, the flow field below the crystal is widely changed with the applied frequency as complete mixing flow, counterclockwise flow and stationary, respectively. Therefore the high frequency magnetic field has not only the same effect as the crystal rotation but also the other effect and this method can be used to control the melt convection. To produce a high quality crystal, however, flat temperature distribution below the crystal and less fluctuation of the temperature field is needed. From this point of view, applied frequency of 500 kHz seems to lead the good result in the case of applied induction coil current of 216 A.

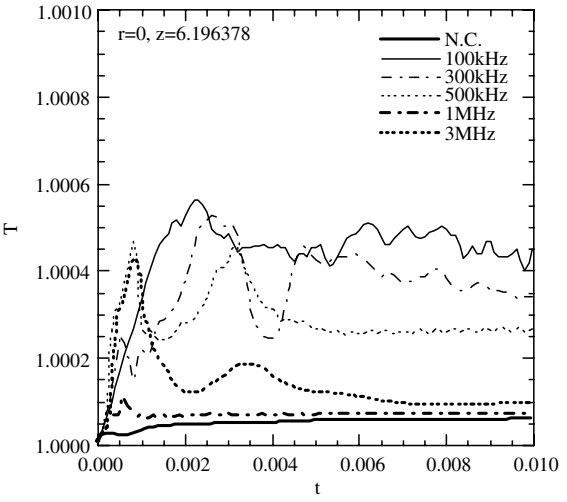

Fig. 6. Melt temperature variation near the center of the crystal for various applied frequency under the applied induction coil current of 216 A.

Next, the effect of applied induction coil current on the melt convection is considered under the fixed applied frequency of 500 kHz. Fig. 7 shows the effect of applied induction coil current on the flow and temperature fields in the CZ silicon melt at $t = 0.01$. The effect of high frequency magnetic field is negligibly small in the case of applied induction coil current of 43.2 A (Fig. 7(a)). If the induction coil current is increased to 86.4 A (Fig. 7(b)), the high frequency magnetic field begins to affect the flow field. However, the counterclockwise flow, which is induced below the crystal, is weak. The region of the counterclockwise flow is enlarged if the induction coil current is increased to 129.6 A (Fig. 7(c)) and such convection prevails in the whole melt region under the induction coil current of 172.8 A (Fig. 7(d)). The temperature field is affected by the melt convection and almost the flat isotherm below the crystal is constructed if the induction coil current is increased to 86.4 A or more. Fig. 8 shows the melt temperature variation beneath the center of the crystal for various applied induction coil current. As shown in this figure, the melt temperature begins to fluctuate if the induction coil current is increased to 86.4 A, however, the fluctuation becomes rather small if the induction coil current is increased to 172.8 A or more. Therefore, at least 86.4 A of the induction coil current is needed to construct the flat temperature distribution below the crystal, which is needed to grow a crystal with flat crystal-melt interface shape, and more than 172.8 A is needed for rather small temperature fluctuation to grow a high quality crystal.

On the real crystal growth process, the effect of flow and temperature fluctuation, which could not be eliminated in the numerical simulation, on the crystal quality

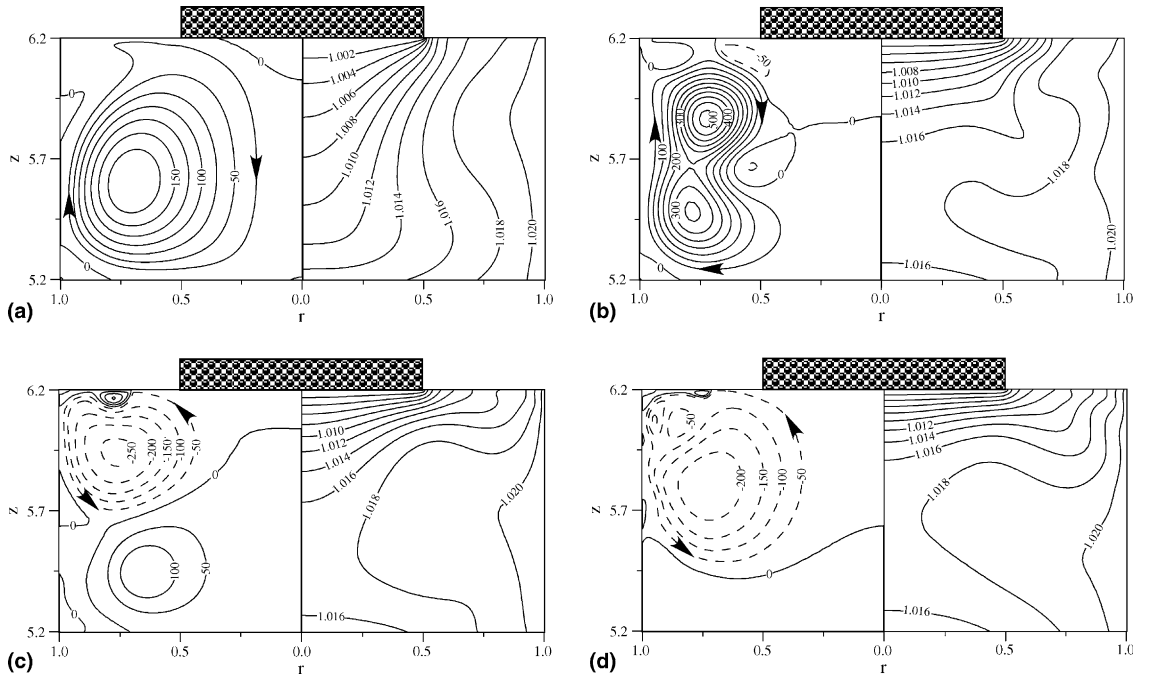

Fig. 7. Effect of applied induction coil current on the flow and temperature fields in the CZ silicon melt under the applied frequency of 500 kHz ($t = 0.01$): (a) 43.2 A; (b) 86.4 A; (c) 129.6 A and (d) 172.8 A.

must be considered. Therefore, not only the effect of high frequency magnetic field on the melt convection but also on the crystal quality should be clarified by an experiment. For this purpose, CZ furnace, which contains the facility of supplying the high frequency magnetic field, is now under construction. The result will come out soon. Since the commonly used crucible diameter in the industries is much bigger than the investigated one, the obtained results cannot be applied directly to the real system. Further investigation should be done in the future.

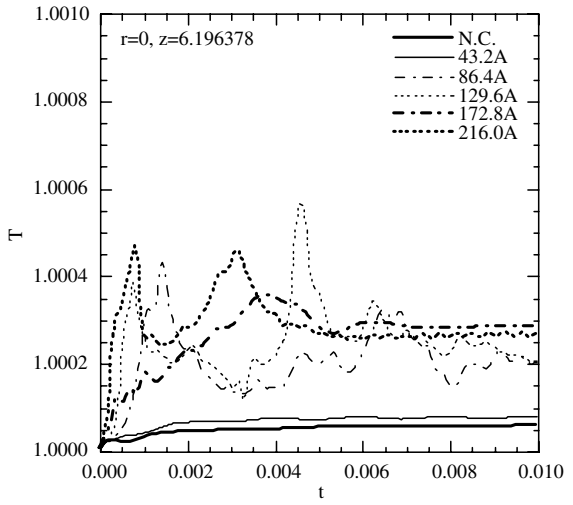

Fig. 8. Melt temperature variation near the center of the crystal for various applied induction coil current under the applied frequency of 500 kHz.

4. Conclusion

To control the CZ silicon melt convection during the single crystal growth process, newly proposed high frequency magnetic field applied method has been investigated numerically and the following results were obtained.

(1) The melt convection is strongly affected by the high frequency magnetic field and the convection structure can be changed by the applied induction coil current and frequency. Therefore, the high frequency magnetic field applied method can also be used as the melt convection control technique.
(2) To achieve a flat temperature distribution below the crystal, less than 500 kHz of the applied frequency and more than 86.4 A of the induction coil current are needed. Further, to obtain the small temperature fluctuation, at least 172.8 A of the induction coil current is needed.
(3) The applicability of this method on the real CZ crystal growth process is still uncertain on the crystal

quality. The effect should be confirmed experimentally.

References

[1] M. Ma, T. Ogawa, M. Watanabe, M. Eguchi, Study on defects in CZ-Si crystals grown under three different cusp magnetic fields by infrared light scattering tomography, J. Cryst. Growth 205 (1999) 50–58.

[2] V.V. Kalaev, D.P. Lukanin, V.A. Zabelin, Yu.N. Makarov, J. Virbulis, E. Dornberger, W. von Ammon, Calculation of bulk defects in CZ Si growth: impact of melt turbulent fluctuations, J. Cryst. Growth 250 (2003) 203–208.

[3] K. Kakimoto, M. Watanabe, M. Eguchi, T. Hibiya, Flow instability of the melt during Czochralski Si crystal growth: dependence on growth conditions; a numerical simulation study, J. Cryst. Growth 139 (1994) 197–205.

[4] K.-W. Yi, K. Kakimoto, M. Eguchi, M. Watanabe, T. Shyo, T. Hibiya, Spoke patterns on molten silicon in Czochralski system, J. Cryst. Growth 144 (1994) 20–28.

[5] K.-W. Yi, V.B. Booker, M. Eguchi, T. Shyo, K. Kakimoto, Structure of temperature and velocity fields in the Si melt of a Czochralski crystal growth system, J. Cryst. Growth 156 (1995) 383–392.

[6] K. Kakimoto, Flow instability during crystal growth from the melt, Prog. Cryst. Growth Charact. 30 (1995) 191–215.

[7] S. Nakamura, M. Eguchi, T. Azami, T. Hibiya, Thermal waves of a nonaxisymmetric flow in a Czochralski-type silicon melt, J. Cryst. Growth 207 (1999) 55–61.

[8] Y. Kishida, K. Okazawa, Geostrophic turbulence in CZ silicon crucible, J. Cryst. Growth 198/199 (1999) 135–140.

[9] D. Vizman, O. Gräbner, G. Müller, Three-dimensional simulation of thermal convection in an industrial Czochralski melt: comparison to experimental results, J. Cryst. Growth 233 (2001) 687–698.

[10] I.Yu. Evstratov, V.V. Kalaev, A.I. Zhmakin, Yu.N. Makarov, A.G. Abramov, N.G. Ivanov, E.M. Smirnov, E. Dornberger, J. Virbulis, E. Tomzig, W. von Ammon, Modeling analysis of unsteady three-dimensional turbulent melt flow during Czochralski growth of Si crystals, J. Cryst. Growth 230 (2001) 22–29.

[11] I.Yu. Evstratov, V.V. Kalaev, A.I. Zhmakin, Yu.N. Makarov, A.G. Abramov, N.G. Ivanov, A.G. Korsakov, E.M. Smirnov, E. Dornberger, J. Virbulis, E. Tomzig, W. von Ammon, Numerical study of 3D unsteady melt convection during industrial-scale CZ Si-crystal growth, J. Cryst. Growth 237–239 (2002) 1757–1761.

[12] N. Nikitin, V. Polezhaev, Direct simulations and stability analysis of the gravity driven convection in a Czochralski model, J. Cryst. Growth 230 (2001) 30–39.

[13] T. Azami, S. Nakamura, M. Eguchi, T. Hibiya, The role of surface-tension-driven flow in the formation of a surface pattern on a Czochralski silicon melt, J. Cryst. Growth 233 (2001) 99–107.

[14] H. Nakanishi, M. Watanabe, K. Terashima, Dependence of Si melt flow in a crucible on surface tension variation in the Czochralski process, J. Cryst. Growth 236 (2002) 523–528.

[15] V. Kumar, B. Basu, S. Enger, G. Brenner, F. Durst, Role of Marangoni convection in Si-Czochralski melts, part I: 3D predictions without crystal, J. Cryst. Growth 253 (2003) 142–154.

[16] V. Kumar, B. Basu, S. Enger, G. Brenner, F. Durst, Role of Marangoni convection in Si-Czochralski melts—part II: 3D predictions with crystal rotation, J. Cryst. Growth 255 (2003) 27–39.

[17] V. Kumar, G. Biswas, G. Brenner, F. Durst, Effect of thermocapillary convection in an industrial Czochralski crucible: numerical simulation, Int. J. Heat Mass Transfer 46 (2003) 1641–1652.

[18] Y.-R. Li, N. Imaishi, T. Azami, T. Hibiya, Three-dimensional oscillatory flow in a thin annular pool of silicon melt, J. Cryst. Growth 260 (2004) 28–42.

[19] Y.-R. Li, Y. Akiyama, N. Imaishi, T. Tsukada, Global analysis of a small Czochralski furnace with rotating crystal and crucible, J. Cryst. Growth 255 (2003) 81–92.

[20] D.T.J. Hurle, R.W. Series, Use of a magnetic field in melt growth, in: D.T.J. Hurle (Ed.), Hand Book of Crystal Growth, 2A, Elsevier Science, Amsterdam, 1994, pp. 259–285.

[21] M. Watanabe, K.W. Yi, T. Hibiya, K. Kakimoto, Direct observation and numerical simulation of molten silicon flow during crystal growth under magnetic fields by X-ray radiography and large-scale computation, Prog. Cryst. Growth Charact. 38 (1999) 215–238.

[22] D. Vizman, J. Friedrich, G. Müller, Comparison of the predictions from 3D numerical simulation with temperature distributions measured in Si Czochralski melts under the influence of different magnetic fields, J. Cryst. Growth 230 (2001) 73–80.

[23] V. Savolainen, J. Heikonen, J. Ruokolainen, O. Anttila, M. Laakso, J. Paloheimo, Simulation of large-scale silicon melt in magnetic Czochralski growth, J. Cryst. Growth 243 (2002) 243–260.

[24] M. Akamatsu, M. Higano, H. Ozoe, Elliptic temperature contours under a transverse magnetic field computed for a Czochralski melt, Int. J. Heat Mass Transfer 44 (2001) 3253–3264.

[25] Y.-S. Lee, Ch.-H. Chun, Effect of a cusp magnetic field on the oscillatory convection coupled with crucible rotation in Czochralski crystal growth, J. Cryst. Growth 197 (1999) 307–316.

[26] D. Vizman, O. Gräbner, G. Müller, 3D numerical simulation and experimental investigations of melt flow in an Si Czochralski melt under the influence of a cusp-magnetic field, J. Cryst. Growth 236 (2002) 545–550.

[27] Y.-R. Li, D.-F. Ruan, N. Imaishi, S.-Y. Wu, L. Peng, D.-L. Zeng, Global simulation of a silicon Czochralski furnace in an axial magnetic field, Int. J. Heat Mass Transfer 46 (2003) 2887–2898.

[28] M. Salk, M. Fiederle, K.W. Benz, A.S. Senchenkov, A.V. Egorov, D.G. Matioukhin, CdTe and $CdTe_{0.9}Se_{0.1}$ crystals grown by the travelling heater method using a rotating magnetic field, J. Cryst. Growth 138 (1994) 161–167.

[29] K.-H. Spitzer, Application of rotating magnetic fields in Czochralski crystal growth, Prog. Cryst. Growth Charact. 38 (1999) 39–58.

[30] M. Watanabe, M. Eguchi, W. Wang, T. Hibiya, S. Kuragaki, Controlling oxygen concentration and distribution in 200 mm diameter Si crystals using the electromag-

netic Czochralski (EMCZ) method, J. Cryst. Growth 237–239 (2002) 1657–1662.
[31] K. Kakimoto, A. Tashiro, T. Shinozaki, H. Ishii, Y. Hashimoto, Mechanisms of heat and oxygen transfer in silicon melt in an electromagnetic Czochralski system, J. Cryst. Growth 243 (2002) 55–65.
[32] Th. Wetzel, A. Muiznieks, A. Mühlbauer, Y. Gelfgat, L. Gorbunov, J. Virbulis, E. Tomzig, W.v. Ammon, Numerical model of turbulent CZ melt flow in the presence of AC and CUSP magnetic fields and its verification in a laboratory facility, J. Cryst. Growth 230 (2001) 81–91.
[33] J. Virbulis, Th. Wetzel, A. Muiznieks, B. Hanna, E. Dornberger, E. Tomzig, A. Mühlbauer, W.v. Ammon, Numerical investigation of silicon melt flow in large diameter CZ-crystal growth under the influence of steady and dynamic magnetic fields, J. Cryst. Growth 230 (2001) 92–99.
[34] T. Munakata, S. Someya, I. Tanasawa, Suppression of Marangoni convection in the FZ melt by high-frequency magnetic field, J. Cryst. Growth 235 (2002) 167–172.
[35] T. Munakata, S. Someya, I. Tanasawa, Effect of high frequency magnetic field on FZ silicon melt convection, in: Proceedings of the 12th International Heat Transfer Conference, 2002, CD-ROM.
[36] T. Kawamura, K. Kuwahara, Computation of high Reynolds number flow around a circular cylinder with surface roughness, AIAA Paper 84–0340 (1984) 9–12.
[37] P. Hintz, D. Schwabe, H. Wilke, Convection in a Czochralski crucible—Part 1: non-rotating crystal, J. Cryst. Growth 222 (2001) 343–355.
[38] X. Wu, K. Kakimoto, H. Ozoe, Z. Guo, Numerical study of natural convection in Czochralski crystallization, Chem. Eng. J. 71 (1998) 183–189.